Genome wide association analysis in a mouse advanced intercross line

Authors: Natalia M. Gonzales[1], Jungkyun Seo[1,2,3], Ana Isabel Hernandez-Cordero[4], Celine L. St. Pierre[1,5], Jennifer S. Gregory[4], Margaret G. Distler[1], Mark Abney[1], Stefan Canzar[1,8], Arimantas Lionikas[4], and Abraham A. Palmer[6,7]

Corresponding author: Abraham A. Palmer; aapalmer@ucsd.edu
ORCID: orcid.org/0000-0003-3634-0747

Affiliations
1. Department of Human Genetics, University of Chicago, Chicago, IL 60637, USA
2. Computational Biology & Bioinformatics Graduate Program, Duke University, Durham, NC, 27708, USA
3. Center for Genomic & Computational Biology, Duke University, Durham, NC, 27708, USA
4. School of Medicine, Medical Sciences and Nutrition, College of Life Sciences and Medicine, University of Aberdeen, Aberdeen, UK
5. Department of Genetics, Washington University School of Medicine, St. Louis, MO 63108, USA
6. Department of Psychiatry, University of California San Diego, La Jolla, CA 92093, USA
7. Institute for Genomic Medicine, University of California San Diego, La Jolla, CA 92093, USA
8. Gene Center, Ludwig-Maximilians-Universität München, 81377 Munich, Germany

Abstract

1
2
3   The LG/J x SM/J advanced intercross line of mice (**LG x SM AIL**) is a multigenerational outbred
4   population. High minor allele frequencies, a simple genetic background, and the fully sequenced LG and
5   SM genomes make it a powerful population for genome-wide association studies. Here we use 1,063 AIL
6   mice to identify 126 significant associations for 50 traits relevant to human health and disease. We also
7   identify thousands of *cis*- and *trans*-eQTLs in the hippocampus, striatum, and prefrontal cortex of ~200
8   mice. We replicate an association between locomotor activity and *Csmd1*, which we identified in an
9   earlier generation of this AIL, and show that *Csmd1* mutant mice recapitulate the locomotor phenotype.
10 Our results demonstrate the utility of the LG x SM AIL as a mapping population, identify numerous novel
11 associations, and shed light on the genetic architecture of mammalian behavior.

Introduction

12

13   Genome-wide association studies (**GWAS**) have revolutionized psychiatric genetics; however,
14 they have also presented numerous challenges. Some of these challenges can be addressed by using
15 model organisms. For example, human GWAS are confounded by environmental variables, such as
16 childhood trauma, which can reduce power to detect genetic associations. In model organisms,
17 environmental variables can be carefully controlled. Furthermore, it has become clear that phenotypic
18 variation in humans is due to numerous common and rare variants of small effect. In model organisms,
19 genetic diversity can be controlled such that all variants are common. In addition, allelic effect sizes in
20 model organisms are dramatically larger than in humans[1,2]. Because the majority of associated loci are in
21 noncoding regions, expression quantitative trait loci (**eQTLs**) are useful for elucidating underlying
22 molecular mechanisms[3,4]. However, it remains challenging to obtain large, high quality samples of
23 human tissue, particularly from the brain. In contrast, tissue for gene expression studies can be collected
24 from model organisms under optimal conditions. Finally, the genomes of model organisms can be edited
25 to assess the functional consequences of specific mutations.
26   Unlike classical F_2 crosses, outbred animals provide improved mapping resolution for GWAS.
27 This is because outbred populations have higher levels of recombination, meaning only markers very
28 close to the causal allele will be associated with the phenotype. However, there is a necessary tradeoff
29 between mapping resolution and statistical power, and this is further aggravated when the causal allele is
30 rare, which is sometimes the case in commercially outbred mice[5,6]. In an effort to combine the resolution
31 afforded by an outbred population with the power of an F_2 cross, we performed GWAS using an
32 advanced intercross line (**AIL**) of mice. Originally proposed by Darvasi and Soller (1995)[7], AILs are the
33 simplest possible outbred population; they are produced by intercrossing two inbred strains beyond the
34 F_2 generation. Because each inbred strain contributes equally to an AIL, all variants are common. This
35 avoids the loss of power that results from rare alleles and simplifies phasing and imputation. Each
36 successive generation of intercrossing further degrades linkage disequilibrium (**LD**) between adjacent
37 markers, which improves mapping resolution relative to classical inbred crosses such as F_2s.
38   An AIL derived from the LG/J (**LG**) and SM/J (**SM**) inbred strains was initiated by Dr. James
39 Cheverud at Washington University in St. Louis[8]. In 2006, we established an independent AIL colony
40 with mice from generation 33 at the University of Chicago (**G33**; Jmc:LG,SM-G33). Because the LG and
41 SM founder strains were independently selected for large and small body size, this AIL has frequently
42 been used to study body weight and other metabolic traits[9–12]. LG and SM also exhibit a variety of
43 behavioral differences, and previous studies from our lab have used the LG x SM AIL to fine-map
44 behavioral associations identified in F_2 crosses between LG and SM[13–15].
45   We recently used commercially available outbred CFW mice to perform a GWAS[5]. In this paper,
46 we apply a similar approach to AIL mice, taking advantage of the more favorable allele frequencies and
47 the ability to impute founder haplotypes. Using mice from AIL generations 50-56 (**G50-56**; Aap:LG,SM-
48 G50-56), we investigate novel behavioral traits, including conditioned place preference for
49 methamphetamine (**CPP**), as well as other biomedically important traits including locomotor activity
50 following vehicle and methamphetamine administration, which have been extensively studied for their
51 relevance to drug abuse[16], and prepulse inhibition (**PPI**), which has been studied for several decades as
52 an endophenotype for schizophrenia[17]. We also examine body weight and a constellation of
53 musculoskeletal phenotypes relevant to exercise physiology, which are known to be heritable in this
54 AIL[10,11,18]. In total, we report 52 associations for 33 behavioral traits and 74 associations for 17
55 physiological traits. We use RNA-sequencing (**RNA-seq**) to measure gene expression in three brain
56 regions of ~200 mice and identify thousands of *cis*- and *trans*-eQTLs, which we use to identify
57 quantitative trait genes (**QTGs**). Finally, we use a mutant mouse line to validate one of our strongest
58 candidate QTGs. Our work demonstrates that the LG x SM AIL is a powerful tool for genetic analysis and
59 provides a methodological framework for GWAS in multigenerational outbred populations. The numerous
60 associations described in this work benefit the complex trait community by shedding light on the genetic
61 architecture of complex traits in a system with only two founders. Although we present only a subset of
62 our findings in detail, AIL genotype, phenotype and gene expression data, complete with a suite of tools
63 for performing GWAS and related analyses, are publicly available on GeneNetwork.org[19].

Results

64

65   We used genotyping by sequencing (**GBS**) to genotype 1,063 of the 1,123 mice that were
66 phenotyped (60 were not successfully genotyped for technical reasons described in the **Supplementary**
67 **Information**). After quality control, GBS yielded 38,238 high-quality autosomal SNPs. Twenty-four AIL
68 mice were also genotyped using the Giga Mouse Universal Genotyping Array[20] (**GigaMUGA**), which
69 yielded only 24,934 polymorphic markers (**Supplementary Fig. 1**). LG and SM have been re-
70 sequenced[21], which allowed us to use the GBS genotypes to impute an additional 4.3 million SNPs (**Fig.
71 1a**). Consistent with the expectation for an AIL, the average minor allele frequency (**MAF**) was high (**Fig.
72 1b**). We also observed that the decay of LD, which is critical to mapping resolution, has increased since
73 the 34th generation (**Fig. 1c**).

LOCO-LMM effectively reduces the type II error rate

75   Linear mixed models (**LMMs**) are now commonly used to perform GWAS in populations that
76 include close relatives because they can incorporate a genetic relationship matrix (**GRM**) that models the
77 covariance of genotypes and phenotypes in samples of related individuals[22]. If SNP data are used to
78 obtain the GRM, this can lead to an inflation of the type II error rate due to proximal contamination[23,24].
79 We have proposed using a leave-one-chromosome-out LMM (**LOCO-LMM**) to address this issue[23]. To
80 demonstrate the appropriateness of a LOCO-LMM, we performed a GWAS for albinism, which is known
81 to be a recessive Mendelian trait caused by the Tyr^c allele, using all three approaches: a simple linear
82 model, an LMM, and a LOCO-LMM (**Fig. 2**). GWAS using a LOCO-LMM for albinism yielded an
83 association on chromosome 7, which contains the Tyr^c allele (**Fig. 2a**). As expected, a quantile-quantile
84 plot showed that p-values from a genome-wide scan using a linear model, which does not account for
85 relatedness, appeared highly inflated (**Fig. 2b**). This inflation was greatly reduced by fitting a standard
86 LMM, which included SNPs from chromosome 7 in both the fixed and random terms (**Fig. 2c**). The
87 LOCO-LMM, which does not include SNPs from the chromosome being tested in the GRM, showed an
88 intermediate level of inflation (**Fig. 2d**). Was the inflation observed in **Fig. 2b-d** due to true signal, or
89 uncontrolled population structure? To address this question, we repeated these analyses after excluding
90 SNPs on chromosome 7 from the fixed effect (**Fig. 2e-g**). Even in the absence of the causal locus, the
91 simple linear model showed substantial inflation, which can only be explained by population structure
92 (**Fig. 2e**). The standard LMM appeared overly conservative, which we attributed to proximal
93 contamination (**Fig. 2f**). The LOCO-LMM showed no inflation, consistent with the absence of Tyr^c and
94 linked SNPs in the fixed effect (**Fig. 2g**). These results demonstrate the appropriateness of a LOCO-
95 LMM.

Genetic architecture of complex traits in the LG x SM AIL

97   We used an LD-pruned set of 523,028 autosomal SNPs genotyped in 1,063 mice from LG x SM
98 G50-56 to perform GWAS for 120 traits using a LOCO-LMM (**Fig. 3a**). Although our primary interest was
99 in behavior, we also measured a number of physiological traits that we knew to be heritable in this AIL.
100 We used permutation to define a significance threshold of $p=8.06 \times 10^{-6}$ ($\alpha=0.05$). We did not use a
101 Bonferroni-corrected significance threshold because we have previously shown that permutation
102 adequately controls type I and II error rates[25]. We identified 52 loci associated with 33 behavioral traits
103 and 74 loci associated with 17 physiological traits (**Fig. 3a**, **Supplementary Table 1; Supplementary
104 Fig. 2**).
105   In populations of related individuals, heritability (**h^2**) estimates may differ depending on whether
106 pedigree data or genetic data is used to calculate the GRM[15,22,26]. Pedigree data captures shared
107 environmental effects and epigenetic effects in addition to additive genetic effects. We used GEMMA[27] to
108 estimate h^2 using a GRM calculated from the AIL pedigree ($\hat{h}^2_{Ped}$) and compared the results to h^2
109 estimates obtained using a GRM calculated from 523,028 SNPs ($\hat{h}^2_{SNP}$). Both methods produced higher
110 estimates of h^2 for physiological traits than for behavioral traits (**Supplementary Table 2**), which is
111 consistent with findings in other rodent GWAS[5,6,28]. For behavioral traits (excluding CPP, locomotor
112 sensitization, and habituation to startle, which were not found to have a genetic component), mean $\hat{h}^2_{Ped}$

2

113   was 0.172 (se=0.066) and mean $\hat{h}^2_{SNP}$ was 0.168 (se=0.038). For physiological traits, $\hat{h}^2_{Ped}$ was 0.453
114   (se=0.088) and $\hat{h}^2_{SNP}$ was 0.355 (se=0.045). The lower standard error for $\hat{h}^2_{SNP}$ indicates that it is a more
115   powerful estimator of h^2 than $\hat{h}^2_{Ped}$. $\hat{h}^2_{SNP}$ is displayed for a subset of traits in **Fig. 3b**; a complete list of h^2
116   estimates and their standard errors are reported in **Supplementary Table 2.** In general, traits with higher
117   heritabilities yielded more associations (**Supplementary Fig. 2**). However, there was no relationship
118   between MAF and the percent variance explained by individual loci (**Supplementary Fig. 3**).
119   We expected many of the traits measured in this study to be correlated with one another (as
120   explained in the **Methods** and **Supplementary Note**). Thus, we calculated Pearson correlation
121   coefficients for all pairwise combinations of traits measured in this study (**Supplementary Fig. 4**). We
122   also used GEMMA to estimate the proportion of genetic and environmental variance shared by each pair
123   of traits (**Supplementary Fig. 5**, **Supplementary Table 3**). As expected, behavioral trait correlations
124   were highest for traits measured on the same day, and correlations among body size traits were also
125   high, even for traits measured at different time points. Trait pairs with high heritabilities shared a larger
126   proportion of genetic variance with one another than with traits that had low heritability. Very little
127   shared genetic variance was observed for behavioral-physiological trait pairs, consistent with their
128   generally low trait correlations.

Identification of eQTLs using RNA-seq

130   For a subset of phenotyped and genotyped mice, we used RNA-seq to measure gene expression
131   in the hippocampus (**HIP**; n=208), prefrontal cortex (**PFC**; n=185) and striatum (**STR**; n=169)
132   (**Supplementary Fig. 6**). We used this data to map local eQTLs (located up to 1 Mb from the start and
133   end of each gene), which we refer to as *cis*-**eQTLs**. We identified 2,902 *cis*-eQTLs in HIP, 2,125 *cis*-
134   eQTLs in PFC and 2,054 *cis*-eQTLs in STR; 1,087 *cis*-eQTLs were significant in all three tissues
135   (FDR<0.05; **Supplementary Table 4. Supplementary Fig. 6-7**).
136   We also mapped distal eQTLs (located on a separate chromosome from the gene tested), which
137   we refer to as *trans*-**eQTLs**. We identified 723 HIP *trans*-eQTLs ($p<9.01\times10^{-6}$), 626 PFC *trans*-eQTLs
138   ($p<1.04\times10^{-5}$) and 653 STR *trans*-eQTLs ($p<8.68\times10^{-6}$) at a genome-wide significance threshold of
139   α=0.05 after testing 49,642 genes across the three tissues (**Supplementary Fig. 6-7; Supplementary
140   Table 5**). Because our permutation corrects for all SNPs tested for a single gene, but not all for all genes
141   and tissues tested, we would expect 5% of tests to be false positives. Quantile-quantile plots that
142   included all SNPs and all genes in each tissue revealed an excess of low p-values, suggesting the
143   presence of true positive results (**Supplementary Fig. 8**).
144   Previous studies in model organisms have identified *trans*-eQTLs that regulate the expression of
145   many genes[4,29,30]; we refer to these as **master eQTLs** (others have called them '*trans*-bands'). We
146   identified several master eQTLs, including one on chromosome 12 (70.19-73.72 Mb) that was associated
147   with the expression of 97 genes distributed throughout the genome (**Supplementary Fig. 9;
148   Supplementary Table 5**). This locus was present in HIP, but not in PFC or STR.

Integration of GWAS and eQTL results

150   The number of significant associations precludes a detailed discussion of each locus. Instead, we
151   have chosen to present several examples that show how we used various layers of complimentary data
152   to parse among the genes within implicated loci. Manhattan plots for all traits are included in
153   **Supplementary Fig. 2**. In addition, all of our data are available on GeneNetwork.org[19], which is a
154   website that provides statistical tools and an interactive graphical user interface, allowing the user to
155   replicate our results and explore additional results not presented in this paper.
156   Four loci associated with locomotor behavior mapped to the same region on chromosome 17
157   (**Supplementary Table 1; Supplementary Fig. 2**). The narrowest association was for side changes
158   between 15-20 min on day 1 (**D1**) of the CPP test, after mice received an injection of vehicle (p=3.60x10⁻
159   ⁶). Other genome-wide significant associations included total D1 side changes (0-30 min), distance
160   traveled on D1 (0-5 min), and distance traveled after an injection of methamphetamine on D2 (15-20 min;
161   **Supplementary Table 1**). The implicated locus contains a single gene, *Crim1* (cysteine rich
162   transmembrane BMP regulator 1)*,* which had a significant *cis*-eQTL in HIP. Although *Crim1* may appear
163   to be the best candidate to explain the associations with locomotor behavior, two nearby genes, *Qpct*

164 (glutaminyl-peptide cyclotransferase) and *Vit* (vitrin), though physically located outside of the locus, also
165 had *cis*-eQTLs within the region associated with locomotor behavior (**Supplementary Table 4**). The top
166 SNP at this locus (rs108572120) is also a *trans*-eQTL for *Zfas1* expression in STR. *Zfas1 is* a noncoding
167 RNA on chromosome 2 of unknown significance. We therefore consider all four genes candidates for
168 mediating the association between this locus and locomotor behavior.
169   One of the most significant loci we identified was associated with startle response (p=5.28x10^{-10};
170 **Fig. 3**; **Supplementary Fig. 2**). The startle response is a motor reflex that is used to assess
171 neurobiological traits related to behavioral plasticity and sensorimotor processing[17,31]. This result
172 replicated a previous association with startle response from our prior study using G34 AIL mice[14]. We
173 examined GWAS p-values for the most significantly associated startle SNP (rs33094557) across all traits
174 that we measured in this study (we refer to this as a phenome-wide association analysis, or **PheWAS**[32]),
175 which revealed that this region pleiotropically affected multiple other traits, including locomotor activity
176 following saline and methamphetamine administration (**Supplementary Fig. 10**). This region was also
177 implicated in conditioned fear and anxiety in prior studies of G34 mice[15], demonstrating that it has
178 extensive pleiotropic effects on behavior. Because the association with startle identifies a relatively large
179 haplotype that included over 25 genes with eQTLs, the causal gene(s) is not clear, and we are not
180 certain whether the pleiotropic effects are due to one or several genes in this interval. In this case, the
181 mapping resolution we obtained was insufficient to address these questions.
182   We also identified a 0.49-Mb locus on chromosome 8 that was associated with locomotor activity
183 (**Fig. 4a; Supplementary Table 1**); this region was nominally associated with PPI and multiple other
184 locomotor traits (**Fig. 4b**). The region identified in the present study (**Fig. 4a-c**) replicates a finding from
185 our previous study using G34 AIL mice[13] (**Fig. 4d**). In both cases, the SM allele conferred increased
186 activity (**Fig. 4c,d**) and the implicated locus contained only one gene: *Csmd1* (CUB and sushi multiple
187 domains 1; **Fig. 4b; Supplementary Table 2**); furthermore, the only *cis*-eQTL that mapped to this region
188 was for *Csmd1* (**Supplementary Fig. 11**). We obtained mice in which the first exon of *Csmd1* was
189 deleted to test the hypothesis that *Csmd1* is the QTG for this locus. *Csmd1* mutant mice exhibited
190 increased activity compared to heterozygous and wild-type mice (**Fig. 4e**), similar to the SM allele. Taken
191 together these data strongly suggest that *Csmd1* is the causal gene.
192   We identified seven overlapping loci for locomotor activity on chromosome 4 (**Supplementary**
193 **Table 1; Supplementary Fig. 2**). The strongest locus (D5 activity, 0-30 min; p=6.75x10^{-9}) spanned 2.31
194 Mb and completely encompassed the narrowest locus, which spanned 0.74 Mb (D5 activity, 25-30 min;
195 p=4.66x10^{-8}); therefore, we focused on the smaller region. *Oprd1* (opioid receptor delta-1) had a *cis*-
196 eQTL in all three brain regions; the SM allele conferred an increase in locomotor activity and was
197 associated with decreased expression of *Oprd1. Oprd1* knockout mice have been reported to display
198 increased activity relative to wild-type mice[33], suggesting that differential expression of *Oprd1* could
199 explain the locomotor effect at this locus. However, we note that there are several other genes and
200 eQTLs within this locus that could also contribute to its behavioral effects.
201   Finally, we identified an association with D1 locomotor behavior on chromosome 6 at
202 rs108610974, which is located in an intron of *Itpr1* (inositol 1,4,5-trisphosphate receptor type 1;
203 **Supplementary Fig. 12**). This locus contained three *cis*-eQTL genes and seven *trans*-eQTLs
204 (**Supplementary Fig. 12**). One of the *trans*-eQTL genes targeted by the locus (*Capn5;* calpain 5) was
205 most strongly associated with rs108610974 and may be the QTG (**Supplementary Table 5**). These
206 results illustrate how knowledge of both *cis*- and *trans*-eQTLs informed our search for QTGs.

Pleiotropic effects on physiological traits

208   Because LG and SM were created by selective breeding for large and small body size, this AIL is
209 expected to segregate numerous body size alleles[9,10]. We measured body weight at ten timepoints
210 throughout development and identified 46 associations, many of which converged at the same loci
211 (**Supplementary Table 1, Supplementary Fig. 2**). For example, eight body weight timepoints were
212 associated with a locus on chromosome 2. Counter to expectations, the LG allele at this locus was
213 associated with *smaller* body mass (**Supplementary Table 1; Supplementary Fig. 2, Supplementary**
214 **Fig. 13**). The narrowest region spanned 0.08 Mb, and while it did not contain any genes, it did contain a
215 *cis*-eQTL SNP for *Nr4a2* (nuclear receptor subfamily 4, group A, member 2) in PFC. Mice lacking *Nr4a2*
216 in midbrain dopamine neurons exhibit a 40% reduction in body weight[34]. Consistent with this, the LG

4

217 allele was associated with decreased expression of *Nr4a2*. Taken together, these data strongly implicate
218 *Nr4a2* as the QTG for this locus.
219   LG and SM also exhibit differences in fat and muscle weight, bone density, and other
220 morphometric traits[9–11,35]. Therefore, we measured the weight of five hind limb muscles, tibia length, and
221 tail length (**Methods**). We identified 22 associations for muscle weight and five for bone length
222 (**Supplementary Table 1**). Six muscle weight loci and one tibia length locus overlapped with
223 associations for body weight. Since body weight, muscle weight, and bone length are interdependent
224 traits, it is difficult to know whether this overlap is due to these traits being correlated (**Supplementary
225 Fig. 4-5, Supplementary Table 3**) or if the causal SNP(s) affect these traits through independent
226 mechanisms. Thus, we use the term 'pleiotropy' to describe these loci instead of claiming a causal
227 relationship. For example, associations for tibialis anterior (**TA**), gastrocnemius, and plantaris weight
228 overlapped a region on chromosome 7 that was associated with all body weight timepoints that we
229 measured (**Supplementary Fig. 2, Supplementary Fig. 14, Supplementary Table 1**). Although the
230 most significant SNP associated with muscle weight was ~5 Mb downstream of the top body weight
231 SNP, the LG allele was associated with greater weight at both loci (**Supplementary Table 1**). For eight
232 out of ten body weight timepoints, the most significant association fell within *Tpp1* (tripeptidyl peptidase
233 1), which was a *cis*-eQTL gene in all tissues and a *trans*-eQTL gene targeted by the master HIP eQTL on
234 chromosome 12 (**Supplementary Fig. 9**). To our knowledge, *Tpp1* has not been shown to affect body
235 size in mice or humans; however, four other *cis*-eQTL genes in the region have been associated with
236 human body mass index (*Rpl27a, Stk33, Trim66,* and *Tub*)[36,37]. Dysfunction of *Tub* (tubby bipartite
237 transcription factor) causes late-onset obesity in mice, perhaps due to *Tub*'s role in insulin signaling[38]. In
238 addition, several *trans*-eQTL genes map to this interval, including *Gnb1* (G protein subunit beta 1)*,* which
239 forms a complex with *Tub*[39]. Another *trans*-eQTL gene associated with this interval, *Crebbp* (*CREB*
240 binding protein), has been associated with juvenile obesity in human GWAS[34].
241   The strongest association we identified in this study was for EDL weight (p=2.03x10^{-13}) on
242 chromosome 13 (**Fig. 3a , Supplementary Table 1; Supplementary Fig. 15**). An association with
243 gastrocnemius weight provided additional support for the region (p=2.56x10^{-7}; **Supplementary Fig. 2,
244 Supplementary Fig. 15**) and in both cases, the SM allele was associated with increased muscle mass.
245 Each locus spanned less than 0.5 Mb and was flanked by regions of low polymorphism between LG and
246 SM (**Supplementary Fig. 15, Supplementary Table 1**). Two *cis*-eQTL genes within the region,
247 *Trappc13* (trafficking protein particle complex 13) and *Nln* (neurolysin), are differentially expressed in LG
248 and SM soleus[12] and TA[18], with LG exhibiting greater expression of both genes. While there is no known
249 relationship between *Trappc13* and muscle, *Nln* has been shown to play a role in mouse skeletal
250 muscle[40].
251   Finally, we identified an association with EDL, plantaris, and TA weight at another locus on
252 chromosome 4 (**Supplementary Table 1**; **Supplementary Fig. 16**). In all cases, the LG allele was
253 associated with greater muscle weight. The loci for EDL and plantaris spanned ~0.5 Mb, defining a
254 region that contained six genes (**Supplementary Table 1**). The top SNPs for EDL (rs239008301;
255 p=7.88x10^{-13}) and plantaris (rs246489756; p=2.25x10^{-6}) were located in an intron of *Astn2* (astrotactin 2)*,*
256 which is differentially expressed in LG and SM soleus[12]. SM, which exhibits lower expression of *Astn2* in
257 soleus relative to LG[12], has a 16 bp insertion in an enhancer region 6.6 kb upstream of *Astn2*
258 (ENSMUSR00000192783)[21]. Two other genes in this region have been associated with muscle or bone
259 phenotypes traits in the mouse: *Tlr4* (toll-like receptor 4), which harbors one synonymous coding
260 mutation on the SM background (rs13489095) and *Trim32* (tripartite motif-containing 32), which contains
261 no coding polymorphisms between the LG and SM strains.
262

Discussion

264   Crosses among well-characterized inbred strains are a mainstay of model organism genetics.
265 However, F_2 and similar crosses provide poor mapping resolution because the ancestral chromosomes
266 persist as extremely long haplotypes[2,22]. To address this limitation, we and others have used various
267 multigenerational intercrosses, including AILs. Using 1,063 male and female mice from LG x SM G50-56,
268 we confirmed that most variants in the LG x SM AIL had high frequencies and that LD has continued to
269 decay between G34 and G50-56 (**Fig. 1**). We identified 126 loci for traits selected for their relevance to

5

270 human psychiatric and metabolic diseases[9,16,17] (**Fig. 3; Supplementary Table 1; Supplementary Fig.**
271 **2**). These results implicated several specific genes that are corroborated by extant human and mouse
272 genetic data. In particular, we replicated a locus on chromosome 8 that was associated with locomotor
273 activity in the G34 study[13] (**Fig. 4**). We showed that the chromosome 8 locus contained a *cis*-eQTL for
274 *Csmd1* (**Supplementary Fig. 11**), which is the only annotated gene within that locus. Finally, we showed
275 that a genetically engineered *Csmd1* mutant mouse recapitulates the locomotor phenotype, strongly
276 suggesting that *Csmd1* is the QTG.

277   Our previous work with this AIL used mice from LG x SM G34 to fine-map loci identified in an F_2
278 cross between LG and SM; however, the mapping resolution in those studies was limited by a lower
279 number of generations, fewer markers (~3,000 SNPs), a smaller sample size, and a higher proportion of
280 first-degree relatives[10,12–14,18]. In the present study we addressed these limitations. The number of SNPs
281 used in our prior studies was increased by several orders of magnitude by using GBS[41,42] followed by
282 imputation from the sequenced founders[21]. Unlike our previous studies using the G34 AIL, in this study
283 we did not use AIL mice to fine map loci identified in an F_2 cross, but instead used them as both a
284 discovery and fine mapping population.

285   The strategies we used to perform GWAS in the LG x SM AIL were also informed by recent
286 GWAS using outbred CFW mice[5,6]. Although our approach to the AIL was similar to the CFW studies,
287 certain practical considerations, along with the AIL's simpler genetic background, affected the design of
288 this study and its outcomes in important ways. For example, non-sibling CFW mice can be obtained from
289 a commercial vendor, which avoids the expenses of maintaining an AIL colony and reduces the
290 complicating effects that can occur when close relatives are used in GWAS. However, haplotype data
291 from the CFW founders are not available, and many CFW alleles exist at low frequencies, limiting power
292 and introducing genetic noise[5,6]. In contrast, the LG and SM founder strains have been fully sequenced[21]
293 and AIL SNPs have high MAFs, which simplifies imputation of SNPs and founder haplotypes and
294 enhances statistical power[22]. Parker *et al.* (2016) demonstrated that GBS is a cost-effective strategy for
295 genotyping CFW mice[5]; however, in the present study, we took advantage of the fact that in the LG x SM
296 AIL, all alleles that are identical by state are also identical by descent. This allowed us to use imputation
297 to obtain 4.3 million SNPs despite using only about half the sequencing depth that was necessary for
298 CFW mice (**Fig. 1a**). Even before imputation, GBS yielded nearly 50% more informative SNPs compared
299 to the best available SNP genotyping chip[20] at about half the cost (**Supplementary Fig. 1**). Thus, we
300 have shown that the use of GBS in a population with sequenced founders is even more powerful than
301 the analogous approach in CFW mice.

302   The primary goal of this study was to identify the genes that are responsible for the loci implicated
303 in behavioral and physiological traits. We were particularly interested in uncovering genetic factors that
304 influence CPP, which is a well-validated measure of the reinforcing effects of drugs[43]. However, the
305 heritability of CPP in LG x SM G50-56 was not significantly different from zero (**Fig. 3b**). This was
306 unexpected since panels of inbred strains and genetically engineered mutant alleles have been shown to
307 exhibit heritable differences in CPP[43–45]. However, the lack of heritability of CPP was partially consistent
308 with our prior study, which used a higher dose of methamphetamine (2 vs. the 1 mg kg^{-1} used in the
309 present study)[46]. We conclude that the low heritability of CPP likely reflects a lack of relevant genetic
310 variation in this specific population. It is possible that even lower doses of methamphetamine, which
311 might fall on the ascending portion of the dose-response function, would have resulted in higher
312 heritability. Responses to other drugs or different CPP methodology may also have resulted in higher
313 heritability. It is also possible that testing for non-additive genetic effects would have increased the
314 heritability of CPP, but we did not investigate this prospect.

315   In general, trait heritability in the LG x SM AIL (**Fig. 3b, Supplementary Table 2**) was lower than
316 what has been reported in studies that use panels of inbred mouse strains to estimate heritability [47–49].
317 This was expected because environmental effects can be shared within but not between inbred strains,
318 which will produce higher estimates of heritability[26]. In addition, epistatic interactions can contribute to
319 heritability in inbred panels, which leads to higher estimates of heritability[50]. These observations share
320 many similarities with the higher heritabilities obtained using twins compared to chip heritabilities in
321 human studies[26].

322   A subset of traits were measured in both this AIL and our prior CFW study (PPI, startle, and body
323 size). Heritability estimates were very similar between those two populations[5]. Despite this, we identified
324 many more genome-wide significant loci in the current study (126 associations in the AIL compared to 17

325 in CFW at α=0.05). The greater number of significant associations generated in this study may be due to
326 enhanced power that comes with the more favorable distribution of MAFs in the AIL (**Supplementary**
327 **Fig. 3**). Differences in genetic background and the rate of LD decay, which also affect power, may also
328 have contributed to these observations and could account for the lack of overlap among loci associated
329 with PPI, startle and body size in the two populations.
330   Our ability to identify QTGs was critically dependent on mapping resolution in the LG x SM AIL
331 (**Fig. 1c**). However, proximity of a gene to the associated SNP is insufficient to establish causality[4].
332 Therefore, we used RNA-seq to quantify mRNA abundance in three brain regions that are strongly
333 implicated in the behavioral traits that we measured: HIP, PFC and STR. We used these data to identify
334 7,081 *cis*-eQTLs (FDR<0.05) and 2,002 *trans*-eQTLs (α=0.05 for a single gene test) (**Supplementary**
335 **Figs. 6-9, Supplementary Tables 4-5**). In a few cases, loci contained only a single eQTL, but in most
336 cases, multiple *cis*-eQTLs and *trans*-eQTLs mapped to the implicated loci. This highlights an important
337 distinction between GWAS using AILs and GWAS using humans. The ability to identify QTLs and eQTLs
338 depends on genetic diversity, LD decay, and MAFs within the sample, which affect power by increasing
339 or reducing the multiple testing burden. Compared to unrelated human populations, AILs have fewer
340 SNPs, higher levels of LD, and higher MAFs (**Fig. 1**), all of which enhance power. We expected the
341 increase in power conferred by an AIL to be less dramatic for *cis*-eQTLs than for *trans*-eQTLs due to the
342 lower number of SNPs tested. This is because unlike human populations, which segregate far more
343 variants (and thus, many more potential eQTLs), genetic diversity in an AIL is limited to variants
344 segregating in the founder strains. Still, the proportion of eQTLs that were significant in all three brain
345 regions was smaller for *trans*-eQTLs versus *cis*-eQTLs (**Supplementary Fig. 10**), consistent with a
346 larger proportion of the *trans*-eQTLs being false positives. Conversely, this observation could be
347 explained by a high rate of false negatives due to the burden of testing all SNPs (*trans*-eQTLs) versus
348 testing only nearby SNPs (*cis*-eQTLs). Thus, in addition to integrating QTLs with eQTLs, we incorporated
349 data about gene expression in other tissues[12,18], coding SNPs, mutant mice, and human genetic studies
350 to parse among the implicated genes. Although that was broadly similar to the approach we applied to
351 CFW mice, the eQTL sample in this study was more than two times greater. Indeed, to our knowledge,
352 this is the largest eQTL analysis that has been performed in outbred mice.
353   We also used PheWAS to identify pleiotropic effects of several loci identified in this study. In
354 many cases, pleiotropy involved highly correlated traits such as body weight on different days or
355 behavior at different time points within a single day (**Supplementary Figs. 13-14,16**; **Supplementary**
356 **Table 1**). We also observed unexpected examples of pleiotropy, for example, between locomotor activity
357 and gastrocnemius mass on chromosome 4 (**Supplementary Fig. 17**) and between locomotor activity
358 and the startle response on chromosome 12 (**Supplementary Fig. 18**). We observed extensive
359 pleiotropy on chromosome 17 at ~26-30 Mb (**Supplementary Table 1**). In the current study we found
360 that this locus influenced saline- and methamphetamine-induced locomotor activity and startle response
361 (**Supplementary Fig. 10**), and this same region was implicated in anxiety-like behavior[15], contextual and
362 conditioned fear[15], and startle response[14] in previous studies of LG x SM G34, suggesting that the locus
363 has a broad impact on many behavioral traits. These results support the idea that pleiotropy is a
364 pervasive feature in model organisms and provides further evidence of the replicability of the loci
365 identified by this and prior GWAS.
366   Discoveries from human GWAS are often considered preliminary until they are replicated in an
367 independent cohort. There were several associations identified in LG x SM G34 mice that we replicated
368 in G50-56[10–12,14,18], however, other findings from G34 did not replicate in G50-56. Replication of GWAS
369 findings is a complex issue in both human and model organism genetics. Failures to replicate prior
370 results in the current study could be due to methodological differences, as previous studies used slightly
371 different statistical models and used data from both F_2 and F_{34} populations. Alternatively, the failure of
372 some loci to replicate could imply that some of our prior findings, while real, did not explain as much of
373 the variance as we estimated due to a 'winner's curse'. Indeed, even if the effect sizes of the earlier
374 findings were correct, we would still not expect to replicate all of them, since our power to replicate is
375 seldom 100%.
376   In model organisms, it is also possible to replicate an association by directly manipulating the
377 implicated gene. We replicated one behavioral locus identified in this study using the criteria of both
378 human and model organism genetics. We had identified an association with locomotor activity on
379 chromosome 8 using G34 of this AIL[13], which was replicated in the present study (**Fig. 4**). In both cases,

380 the SM allele was associated with lower activity (**Fig. 4c-d**). We also identified a locus for PPI (76 dB) in
381 this region (**Fig. 4a**; **Supplementary Table 1, Supplementary Fig. 2**). The loci identified in both G34
382 and in G50-56 were small and contained just one gene: *Csmd1* (**Fig. 4b**). In the present study, we also
383 identified a *cis*-eQTL for *Csmd1* in HIP (**Supplementary Fig. 11**). Finally, we obtained *Csmd1* mutant
384 mice[51] that also exhibited altered locomotor activity (**Fig. 4e**). Thus, we have demonstrated replication
385 both by performing an independent GWAS and by performing an experimental manipulation that
386 recapitulates the phenotype.
387   In summary, we have shown that LG x SM AIL mice are a powerful multigenerational intercross
388 population that can be used for GWAS. The simple genetic background of an AIL makes it an appealing
389 alternative to other multigenerational mouse populations, such as the Diversity Outcross[52]. We have
390 identified numerous genome-wide significant loci for a variety of biomedically significant phenotypes. We
391 also made use of eQTL data to parse among the genes implicated in particular loci. In the case of
392 *Csmd1*, we showed replication in a second mapping population and by directly manipulating the
393 implicated gene, which produced a similar phenotype.
394
395

Methods

Genetic background

398   The LG and SM inbred strains were independently selected for high and low body weight at 60
399 days[53]. The LG x SM AIL was derived from an F_1 intercross of SM females and LG males initiated by Dr.
400 James Cheverud at Washington University in St. Louis[8]. Subsequent AIL generations were maintained
401 using at least 65 breeder pairs selected by pseudo-random mating[54]. In 2006, we established an
402 independent AIL colony using 140 G33 mice obtained from Dr. Cheverud (Jmc: LG,SM-G33). Since
403 2009, we have selected breeders using an R script that leverages pairwise kinship coefficients estimated
404 from the AIL pedigree to select the most unrelated pairs while also attempting to minimize mean kinship
405 among individuals in the incipient generation (the full pedigree is included in **Supplementary Data** and a
406 link to the R script is in the **Supplementary Note**). We maintained ~100 breeder pairs in G49-55 to
407 produce the mice for this study. In each generation, we used one male and one female from each
408 nuclear family for phenotyping and reserved up to three of their siblings for breeding the next generation.

Phenotypes

410   We subjected 1,123 AIL mice (562 female, 561 male; Aap: LG,SM-G50-56) to a four-week battery
411 of tests over the course of two years. 1,063 of these mice (530 female, 533 male) had high-quality GBS
412 data; therefore, we restricted our analysis to these individuals. This sample size was based on an
413 analysis suggesting that 1,000 mice would provide 80% power to detect associations explaining 3% of
414 the phenotypic variance (**Supplementary Fig. 19**). We measured CPP for 1 mg kg^{-1} methamphetamine,
415 locomotor behavior, PPI, startle, body weight, muscle mass, bone length and other related traits
416 (**Supplementary Table 2**). We tested mice during the light phase of a 12:12h light-dark cycle in 22
417 batches comprised of 24-71 individuals (median=53.5). Median age was 54 days (mean=55.09,
418 range=35-101) at the start of testing and 83 days (mean=84.4, range=64-129) at death. Standard lab
419 chow and water were available *ad libitum*, except during testing. Testing was performed during the light
420 phase, starting one hour after lights on and ending one hour before lights off. No environmental
421 enrichment was provided. All procedures were approved by the Institutional Animal Care and Use
422 Committee at the University of Chicago. Traits are summarized briefly below; detailed descriptions are
423 provided in the **Supplementary Methods.**
424   **CPP and locomotor behavior**: CPP is an associative learning paradigm that has been used to
425 measure the motivational properties of drugs in humans[55] and rodents[43]. We defined CPP as the number
426 of seconds spent in a drug-associated environment relative to a neutral environment over the course of
427 30 minutes. The full procedure takes eight days, which we refer to as **D1-D8**. We measured baseline
428 preference after administration of vehicle (0.9% saline, i.p.) on D1. On D2 and D4, mice were

429 administered methamphetamine (1 mg kg^{-1}, i.p.) and restricted to one visually and tactically distinct
430 environment; on D3 and D5 mice were administered vehicle and restricted to the other, contrasting
431 environment. No testing occurs on D6 and D7. On D8, mice were allowed to choose between the two
432 environments after administration of vehicle; we measured CPP at this time. Other variables measured
433 during the CPP test include the distance traveled (cm) on all testing days, the number of side changes on
434 D1 and D8, and locomotor sensitization to methamphetamine (the increase in activity on D4 relative to
435 D2). We measured CPP and locomotor traits across six five-minute intervals and summed them to
436 generate a total phenotype for each day.
437   **PPI and startle**: PPI is the reduction of the acoustic startle response when a loud noise is
438 immediately preceded by a low decibel (**dB**) prepulse[56]. PPI and startle are measured across multiple
439 trials that occur over four consecutive blocks of time[14]. The primary startle trait is the mean startle
440 amplitude across all pulse-alone trials in blocks 1-4. Habituation to startle is the difference between the
441 mean startle response at the start of the test (block 1) and the end of the test (block 4). PPI, which we
442 measured at three prepulse intensities (3, 6, and 12 dB above 70 dB background noise), is the mean
443 startle response during pulse-alone trials in blocks 2-3 normalized by the mean startle response during
444 prepulse trials in blocks 2-3. Mice that exhibited a startle response in the absence of a pulse were
445 excluded from GWAS, as were mice that did *not* exhibit a startle response during the first block of startle
446 pulses (**Supplementary Methods, Supplementary Fig. 20**).
447   **Physiological traits:** We measured body weight (g) on each testing day and at the time of death.
448 One week after PPI, we measured blood glucose levels (mg/dL) after a four-hour fast. One week after
449 glucose testing, we killed the mice, and measured tail length (cm from base to tip of the tail). We stored
450 spleens in a 1.5 mL solution of 0.9% saline at -80°C until DNA extraction. We removed the left hind limb
451 of each mouse just below the pelvis; hind limbs were stored at -80°C. Frozen hind limbs were
452 phenotyped by Dr. Arimantas Lionikas at the University of Aberdeen. Phenotyped muscles include two
453 dorsiflexors, TA and EDL, and three plantar flexors: gastrocnemius, plantaris and soleus. We isolated
454 individual muscles under a dissection microscope and weighed them to 0.1 mg precision on a Pioneer
455 balance (Ohaus, Parsippany, NJ, USA). After removing soft tissue from the length of tibia, we measured
456 its length to 0.01 mm precision with a Z22855 digital caliper (OWIM GmbH & Co., Neckarsulm, GER).
457   **Brain tissue**: We collected HIP, PFC and STR for RNA-seq from the brain of one mouse per
458 cage. This allowed us to dissect each brain within five minutes of removing a cage from the colony room
459 (rapid tissue collection was intended to limit stress-induced changes in gene expression). We
460 preselected brain donors to prevent biased sampling of docile (easily caught) mice and to avoid sampling
461 full siblings, which would reduce our power to detect eQTLs. Intact brains were extracted and submerged
462 in chilled RNALater (Ambion, Carlsbad, CA, USA) for one minute before dissection. Individual tissues
463 were stored separately in chilled 0.5-mL tubes of RNALater. All brain tissue was dissected by the same
464 experimenter and subsequently stored at -80°C until extraction.

GBS variant calling and imputation

466   GBS is a reduced-representation genotyping method[41,57] that we have adapted for use in mice
467 and rats[5,42]. We extracted DNA from spleen using a standard salting-out protocol and prepared GBS
468 libraries by digesting DNA with the restriction enzyme *PstI*. We sequenced 24 uniquely barcoded
469 samples per lane of an Illumina HiSeq 2500 using single-end, 100 bp reads. We aligned 1,110 GBS
470 libraries to the mm10 reference genome before using GATK[58] to realign reads around known indels in
471 LG and SM[21] (**Supplementary Methods**). We obtained an average of 3.2 million reads per sample. We
472 discarded 32 samples with <1 million reads aligned to the main chromosome contigs (1-19, X, Y) or with
473 a primary alignment rate <77% (i.e. three s.d. below the mean of 97.4%; **Supplementary Fig. 21**).
474   We used ANGSD[59] to obtain genotype likelihoods for the remaining 1,078 mice and used
475 Beagle[60,61] for variant calling, which we performed in two stages. We used first-pass variant calls as input
476 for IBDLD[62,63], which we used to estimate kinship coefficients for the mice in our sample. Because our
477 sample contained opposite-sex siblings, we were able to identify and resolve sample mix-ups by
478 comparing genetic kinship estimates to kinship estimated from the LG x SM pedigree (**Supplementary**
479 **Data 1, Supplementary Note**). In addition, we re-genotyped 24 mice on the GigaMUGA[20] to evaluate
480 GBS variant calls (**Supplementary Table 6** lists concordance rates at various stages of our pipeline; see
481 **Supplementary Methods** for details).

9

482   After identifying and correcting sample mix-ups, we discarded 15 samples whose identities could
483   not be resolved (**Supplementary Methods**). Next, we used Beagle[60,61], in conjunction with LG and SM
484   haplotypes obtained from whole-genome sequencing data[21] to impute 4.3 million additional SNPs into
485   the final sample of 1,063 mice. We excluded X chromosome SNPs to avoid potential problems with
486   genotyping accuracy, statistical power, and other complications that have been discussed elsewhere[64].
487   We removed SNPs with low MAFs (<0.1), SNPs with Hardy-Weinberg Equilibrium (**HWE**) violations (p ≤
488   7.62×10^{-6}, determined from gene dropping simulations as described in the **Supplementary Methods**),
489   and SNPs with low imputation quality (dosage r^2, **DR^2** <0.9). We then pruned variants in high LD
490   (r^2>0.95) to obtain the 523,028 SNPs that we used for GWAS.

LD Decay

492   We used PLINK[65] to calculate r^2 for all pairs of autosomal GWAS SNPs typed in G50-56
493   (parameters are listed in **Supplementary Note**). We repeated the procedure for 3,054 SNPs that were
494   genotyped in G34 mice[13]. Next, we randomly sampled r^2 values calculated for ~40,000 SNP pairs from
495   each population and used the data to visualize the rate of LD decay (**Fig. 1c**).

GWAS

497   We used a 'leave one chromosome out' LMM (**LOCO-LMM**) implemented in GEMMA[27] to perform
498   GWAS. An LMM accounts for relatedness by modeling the covariance between phenotypes and
499   genotypes as a random, polygenic effect, which we also refer to as a genetic relationship matrix (**GRM**).
500   Power to detect associations is reduced when the locus being tested is also included in the GRM
501   because the effect of the locus is represented in both the fixed and random terms[13,24]. To address this
502   issue, we calculated 19 separate GRMs, each one excluding a different chromosome. When testing
503   SNPs on a given chromosome, we used the GRM that did not include markers from that chromosome as
504   the polygenic effect in the model. Fixed covariates for each trait are listed in **Supplementary Table 2.**
505   We used a permutation-based approach implemented in MultiTrans[66] and SLIDE[67] to obtain a
506   genome-wide significance threshold that accounts for LD between nearby markers (**Supplementary**
507   **Methods**). We obtained a significance threshold of $p=8.06 \times 10^{-6}$ (α=0.05) from 2.5 million samplings.
508   Because the phenotypic data were quantile-normalized, we applied the same threshold to all traits. We
509   converted p-values to LOD scores and used a 1.5-LOD support interval to approximate a critical region
510   around each associated region, which enabled us to systematically identify overlap with eQTLs.

Trait correlations and heritability

512   We calculated the Pearson correlation coefficients and their p-values for all pairs of traits
513   measured in this study. Only mice with non-missing data for both traits in a pair were used to calculate
514   the correlation. We also decomposed the trait covariance into genetic and environmental covariances
515   using a multivariate LOCO-LMM in GEMMA[68]. This allowed us to evaluate the contribution of genetic and
516   environmental factors to each pair of traits (**Supplementary Fig. 5, Supplementary Table 3**).
517   We estimated the proportion of phenotypic variance explained by the additive effects of 523,028
518   LD-pruned SNPs using the restricted maximum likelihood algorithm in GEMMA[27]. Specifically, we ran a
519   second genome-wide scan for each trait, this time dropping the fixed effect of dosage and including the
520   complete GRM estimated from SNPs on all 19 autosomes. We refer to this estimate as 'SNP heritability'
521   ($\hat{h}^2_{SNP}$). For comparison, we also estimated heritability using pedigree data ($\hat{h}^2_{Ped}$). We used the same
522   method described above, only the GRM was replaced with a kinship matrix estimated from the AIL
523   pedigree (**Supplementary Table 2, Supplementary Note, Supplementary Data 1**). To estimate effect
524   sizes for trait-associated SNPs, we repeated the procedure for $\hat{h}^2_{SNP}$ using dosage at the most significant
525   SNP as a covariate for each trait (**Supplementary Table 1**). We interpreted the difference between the
526   two estimates as the effect size of that locus.

RNA-sequencing and quality control

We extracted RNA from HIP, PFC and STR using a standard phenol-chloroform procedure and prepared cDNA libraries from 741 samples with RNA integrity scores ≥ 8.0 (265 HIP; 240 PFC; 236 STR)[69] as measured on a Bioanalyzer (Agilent, Wilmington, DE, USA). We used Quant-iT kits to quantify RNA (Ribogreen) and cDNA (Picogreen; Fisher Scientific, Pittsburgh, PA, USA). Barcoded sequencing libraries were prepared with the TruSeq RNA Kit (Illumina, San Diego, USA), pooled in sets of 24, and sequenced on two lanes of an Illumina HiSeq 2500 using 100 bp, single-end reads.

Because mapping quality tends to be higher for reads that closely match the reference genome[70], read mapping in an AIL may be biased toward the reference strain (C57BL/6J)[71]. We addressed this concern by aligning RNA-seq reads to custom genomes created from LG and SM using whole-genome sequence data[21]. We used default parameters in HISAT[72] for alignment and GenomicAlignments[73] for assembly, assigning each read to a gene as defined by Ensembl (*Mus_musculus*.GRCm38.85)[74]. We required that each read overlap one unique disjoint region of the gene. If a read contained a region overlapping multiple genes, genes were split into disjoint intervals, and any shared regions between them were hidden. If the read overlapped one of the remaining intervals, it was assigned to the gene that the interval originated from; otherwise, it was discarded. Next, we reassigned the mapping position and CIGAR strings for each read to match mm10 genome coordinates and combined the LG and SM alignment files for each sample by choosing the best mapping. Only uniquely mapped reads were included in the final alignment files. We then used DESeq[75] to obtain normalized read counts for each gene in HIP, PFC and STR. We excluded genes detected in <95% of samples within each tissue. We retained a total of 16,533 genes in HIP, 16,249 genes in PFC, and 16,860 genes in STR.

We also excluded 30 samples with <5M mapped reads or with an alignment rate <91.48% (i.e. less than 1 s.d. below the mean number of reads or the mean alignment rate across all samples and tissues; **Supplementary Fig. 22**). We merged expression data from HIP, PFC and STR and plotted the first two principal components (**PCs**) of the data to identify potential tissue swaps. Most samples clustered into distinct groups based on tissue. We reassigned 12 mismatched samples to new tissues and removed 35 apparently contaminated samples that did not cluster with the rest of the data (**Supplementary Fig. 23**). We also used agreement among GBS genotypes and genotypes called from RNA-seq data in the same individuals to identify and resolve mixed-up samples, as detailed in the **Supplementary Methods.** We discarded 108 sample mix-ups that we were not able to resolve, 29 samples with low-quality GBS data, and 12 outliers (details are provided in the **Supplementary Methods**). A total of 208 HIP, 185 PFC, and 169 STR samples were retained for further analyses.

eQTL mapping

Prior to eQTL mapping, we quantile-normalized gene expression data and used principal components analysis to remove the effects of unknown confounding variables[76]. For each tissue, we calculated the first 100 PCs of the gene expression matrix. We quantile-normalized PCs and used GEMMA[27] to test for association with SNPs using sex and batch as covariates. We evaluated significance with the same permutation-based threshold used for GWAS. We retained PCs that showed evidence of association with a SNP in order to avoid removing *trans*-eQTL effects. We then used linear regression to remove the effects of the remaining PCs (**Supplementary Fig. 24**) and quantile-normalized the residuals.

We then mapped *cis*- and *trans*-eQTLs using a LOCO-LMM implemented in GEMMA[27]. We considered intergenic SNPs and SNPs 1 Mb upstream or downstream of the gene as potential *cis*-eQTLs and excluded 2,143 genes that had no SNPs within their *cis*-regions. We used eigenMT[77] to obtain a gene-based p-value adjusted for the number of independent SNPs in each *cis* region. We declared *cis*-eQTLs significant at an FDR<0.05 (**Supplementary Table 4**).

SNPs on chromosomes that did not contain the gene being tested were considered potential *trans*-eQTLs. We determined significance thresholds for *trans*-eQTLs by permuting the data 1,000 times. Since expression data were quantile-normalized, we permuted one randomly chosen gene per tissue. The significance threshold for *trans*-eQTLs was $p=8.68 \times 10^{-6}$ in STR, $p=9.01 \times 10^{-6}$ in HIP, and $p=1.04 \times 10^{-5}$ in PFC (α=0.05). We used all SNPs for permutation; therefore, we expect these thresholds to be slightly conservative. We define 'master eQTLs' as 5 Mb regions that contain ten or more *trans*-eQTLs. To

11

579 identify master eQTLs, we divided chromosomes into 5 Mb bins and assigned each *trans*-eQTL gene to
580 the bin containing its most significant eQTL SNP.

Csmd1 mutant mice

582 *Csmd1* mutants were created by Lexicon Genetics by inserting a Neomycin cassette into the first
583 exon of *Csmd1* using embryonic stem cells derived from 129S5 mice[78]. The mice we used were the
584 result of a C57BL/6 x 129S5 intercross designated B6;129S5-*Csmd1*[tm1Lex]/Mmucd (the exact C57BL/6
585 substrain is unknown). We bred heterozygous males and females and tested littermate offspring to
586 account for their mixed genetic background. *Csmd1* spans 1.6 Mb and has 70 exons. Its four major
587 transcripts, termed *Csmd1-1* to *Csmd1-4*, are expressed in the central nervous system[51]. Distler *et al.*
588 (ref. 51) demonstrated that *Csmd1* homozygous mutant mice express <30% of wild-type *Csmd1* levels in
589 the brain, and heterozygous mice show a 54% reduction in *Csmd1* expression. Residual expression of
590 *Csmd1* in homozygous mutant mice is derived from *Csmd1-4*, the only transcript that does not include
591 the first exon. We analyzed locomotor behavior on two days following a saline injection in 31 wild-type,
592 59 heterozygous, and 48 mutant mice.

Code availability

594 Example code for running the analyses in this study are provided in the **Supplementary Note.**

Data availability

596 The AIL pedigree is provided as **Supplementary Data 1**. Genotypes, phenotypes and gene
597 expression data from LG x SM G50-56 mice are freely and publicly available to explore on
598 GeneNetwork.org (Study ID 272). Accession codes are GN844-846 for RNAseq data and GN653 for
599 phenotype data. An accession code for genotype data is pending.

References

600 1. Flint, J. & Mackay, T. F. C. Genetic architecture of quantitative traits in mice, flies, and humans.
601   *Genome Res.* **19,** 723–733 (2009).
602 2. Parker, C. C. & Palmer, A. A. Dark matter: are mice the solution to missing heritability? *Front. Genet.*
603   **2,** 32 (2011).
604 3. GTEx Consortium *et al.* Genetic effects on gene expression across human tissues. *Nature* **550,** 204–
605   213 (2017).
606 4. Albert, F. W. & Kruglyak, L. The role of regulatory variation in complex traits and disease. *Nat. Rev.*
607   *Genet.* **16,** 197–212 (2015).
608 5. Parker, C. C. *et al.* Genome-wide association study of behavioral, physiological and gene expression
609   traits in outbred CFW mice. *Nat. Genet.* **48,** 919–926 (2016).
610 6. Nicod, J. *et al.* Genome-wide association of multiple complex traits in outbred mice by ultra low-
611   coverage sequencing. *Nat. Genet.* **48,** 912–918 (2016).
612 7. Darvasi, A. & Soller, M. Advanced intercross lines, an experimental population for fine genetic
613   mapping. *Genetics* **141,** 1199–1207 (1995).
614 8. Ehrich, T. H. *et al.* Fine-mapping gene-by-diet interactions on chromosome 13 in a LGVJ X SMVJ
615   murine model of obesity. *Diabetes* **54,** 1863–1872 (2005).
616 9. Lawson, H. A. & Cheverud, J. M. Metabolic syndrome components in murine models. *Endocr. Metab.*
617   *Immune Disord. Drug Targets* **10,** 25–40 (2010).
618 10. Parker, C. C. *et al.* Fine-mapping alleles for body weight in LG/J X SM/J F2 and F(34) advanced
619   intercross lines. *Mamm. Genome Off. J. Int. Mamm. Genome Soc.* **22,** 563–571 (2011).
620 11. Lionikas, A., Cheng, R., Lim, J. E., Palmer, A. A. & Blizard, D. A. Fine-mapping of muscle weight
621   QTL in LG/J and SM/J intercrosses. *Physiol. Genomics* **42A,** 33–38 (2010).
622 12. Carroll, A. M. *et al.* Fine-mapping of genes determining extrafusal fiber properties in murine soleus
623   muscle. *Physiol. Genomics* **49,** 141–150 (2017).

13. Cheng, R. *et al.* Genome-wide association studies and the problem of relatedness among advanced intercross lines and other highly recombinant populations. *Genetics* **185,** 1033–1044 (2010).

14. Samocha, K. E., Lim, J. E., Cheng, R., Sokoloff, G. & Palmer, A. A. Fine mapping of QTL for prepulse inhibition in LG/J and SM/J mice using F(2) and advanced intercross lines. *Genes Brain Behav.* **9,** 759–767 (2010).

15. Parker, C. C. *et al.* High-resolution genetic mapping of complex traits from a combined analysis of F2 and advanced intercross mice. *Genetics* **198,** 103–116 (2014).

16. de Wit, H. & Phillips, T. J. Do initial responses to drugs predict future use or abuse? *Neurosci. Biobehav. Rev.* **36,** 1565–1576 (2012).

17. Swerdlow, N. R., Braff, D. L. & Geyer, M. A. Sensorimotor gating of the startle reflex: what we said 25 years ago, what has happened since then, and what comes next. *J. Psychopharmacol. Oxf. Engl.* **30,** 1072–1081 (2016).

18. Lionikas, A. *et al.* Resolving candidate genes of mouse skeletal muscle QTL via RNA-Seq and expression network analyses. *BMC Genomics* **13,** 592 (2012).

19. Mulligan, M. K., Mozhui, K., Prins, P. & Williams, R. W. GeneNetwork: A Toolbox for Systems Genetics. *Methods Mol. Biol. Clifton NJ* **1488,** 75–120 (2017).

20. Morgan, A. P. *et al.* The Mouse Universal Genotyping Array: From Substrains to Subspecies. *G3 Bethesda Md* **6,** 263–279 (2015).

21. Nikolskiy, I. *et al.* Using whole-genome sequences of the LG/J and SM/J inbred mouse strains to prioritize quantitative trait genes and nucleotides. *BMC Genomics* **16,** 415 (2015).

22. Gonzales, N. M. & Palmer, A. A. Fine-mapping QTLs in advanced intercross lines and other outbred populations. *Mamm. Genome Off. J. Int. Mamm. Genome Soc.* **25,** 271–292 (2014).

23. Cheng, R., Parker, C. C., Abney, M. & Palmer, A. A. Practical considerations regarding the use of genotype and pedigree data to model relatedness in the context of genome-wide association studies. *G3 Bethesda Md* **3,** 1861–1867 (2013).

24. Listgarten, J. *et al.* Improved linear mixed models for genome-wide association studies. *Nat. Methods* **9,** 525–526 (2012).

25. Cheng, R. & Palmer, A. A. A simulation study of permutation, bootstrap, and gene dropping for assessing statistical significance in the case of unequal relatedness. *Genetics* **193,** 1015–1018 (2013).

26. Yang, J., Zeng, J., Goddard, M. E., Wray, N. R. & Visscher, P. M. Concepts, estimation and interpretation of SNP-based heritability. *Nat. Genet.* **49,** 1304–1310 (2017).

27. Zhou, X. & Stephens, M. Genome-wide efficient mixed-model analysis for association studies. *Nat. Genet.* **44,** 821–824 (2012).

28. Rat Genome Sequencing and Mapping Consortium *et al.* Combined sequence-based and genetic mapping analysis of complex traits in outbred rats. *Nat. Genet.* **45,** 767–775 (2013).

29. Chesler, E. J. *et al.* Complex trait analysis of gene expression uncovers polygenic and pleiotropic networks that modulate nervous system function. *Nat. Genet.* **37,** 233–242 (2005).

30. Hasin-Brumshtein, Y. *et al.* Hypothalamic transcriptomes of 99 mouse strains reveal trans eQTL hotspots, splicing QTLs and novel non-coding genes. *eLife* **5,** (2016).

31. Koch, M. The neurobiology of startle. *Prog. Neurobiol.* **59,** 107–128 (1999).

32. Bush, W. S., Oetjens, M. T. & Crawford, D. C. Unravelling the human genome-phenome relationship using phenome-wide association studies. *Nat. Rev. Genet.* **17,** 129–145 (2016).

33. Filliol, D. *et al.* Mice deficient for delta- and mu-opioid receptors exhibit opposing alterations of emotional responses. *Nat. Genet.* **25,** 195–200 (2000).

34. Kadkhodaei, B. *et al.* Nurr1 is required for maintenance of maturing and adult midbrain dopamine neurons. *J. Neurosci. Off. J. Soc. Neurosci.* **29,** 15923–15932 (2009).

35. Carroll, A. M., Palmer, A. A. & Lionikas, A. QTL Analysis of Type I and Type IIA Fibers in Soleus Muscle in a Cross between LG/J and SM/J Mouse Strains. *Front. Genet.* **2,** 99 (2011).

36. Locke, A. E. *et al.* Genetic studies of body mass index yield new insights for obesity biology. *Nature* **518,** 197–206 (2015).

37. Berndt, S. I. *et al.* Genome-wide meta-analysis identifies 11 new loci for anthropometric traits and provides insights into genetic architecture. *Nat. Genet.* **45,** 501–512 (2013).

13

677   38. Stretton, C., Litherland, G. J., Moynihan, A., Hajduch, E. & Hundal, H. S. Expression and modulation
678   of TUB by insulin and thyroid hormone in primary rat and murine 3T3-L1 adipocytes. *Biochem.*
679   *Biophys. Res. Commun.* **390,** 1328–1333 (2009).
680   39. Baehr, W. & Frederick, J. M. Naturally occurring animal models with outer retina phenotypes. *Vision*
681   *Res.* **49,** 2636–2652 (2009).
682   40. Cavalcanti, D. M. L. P. *et al.* Neurolysin knockout mice generation and initial phenotype
683   characterization. *J. Biol. Chem.* **289,** 15426–15440 (2014).
684   41. Elshire, R. J. *et al.* A robust, simple genotyping-by-sequencing (GBS) approach for high diversity
685   species. *PloS One* **6,** e19379 (2011).
686   42. Fitzpatrick, C. J. *et al.* Variation in the form of Pavlovian conditioned approach behavior among
687   outbred male Sprague-Dawley rats from different vendors and colonies: sign-tracking vs. goal-
688   tracking. *PloS One* **8,** e75042 (2013).
689   43. Tzschentke, T. M. Measuring reward with the conditioned place preference (CPP) paradigm: update
690   of the last decade. *Addict. Biol.* **12,** 227–462 (2007).
691   44. Philip, V. M. *et al.* High-throughput behavioral phenotyping in the expanded panel of BXD
692   recombinant inbred strains. *Genes Brain Behav.* **9,** 129–159 (2010).
693   45. Martinelli, D. C. *et al.* Expression of C1ql3 in Discrete Neuronal Populations Controls Efferent
694   Synapse Numbers and Diverse Behaviors. *Neuron* **91,** 1034–1051 (2016).
695   46. Bryant, C. D., Kole, L. A., Guido, M. A., Cheng, R. & Palmer, A. A. Methamphetamine-induced
696   conditioned place preference in LG/J and SM/J mouse strains and an F45/F46 advanced intercross
697   line. *Front. Genet.* **3,** 126 (2012).
698   47. Mhyre, T. R. *et al.* Heritability, correlations and in silico mapping of locomotor behavior and
699   neurochemistry in inbred strains of mice. *Genes Brain Behav.* **4,** 209–228 (2005).
700   48. Iraqi, F. A. *et al.* Heritability and coefficient of genetic variation analyses of phenotypic traits provide
701   strong basis for high-resolution QTL mapping in the Collaborative Cross mouse genetic reference
702   population. *Mamm. Genome Off. J. Int. Mamm. Genome Soc.* **25,** 109–119 (2014).
703   49. Liu, X. & Gershenfeld, H. K. Genetic differences in the tail-suspension test and its relationship to
704   imipramine response among 11 inbred strains of mice. *Biol. Psychiatry* **49,** 575–581 (2001).
705   50. Bennett, B. J. *et al.* Genetic Architecture of Atherosclerosis in Mice: A Systems Genetics Analysis of
706   Common Inbred Strains. *PLoS Genet.* **11,** e1005711 (2015).
707   51. Distler, M. G., Opal, M. D., Dulawa, S. C. & Palmer, A. A. Assessment of behaviors modeling
708   aspects of schizophrenia in Csmd1 mutant mice. *PloS One* **7,** e51235 (2012).
709   52. Chesler, E. J. *et al.* Diversity Outbred Mice at 21: Maintaining Allelic Variation in the Face of
710   Selection. *G3 Bethesda Md* **6,** 3893–3902 (2016).
711   53. Beck, J. A. *et al.* Genealogies of mouse inbred strains. *Nat. Genet.* **24,** 23–25 (2000).
712   54. Ehrich, T. H., Kenney-Hunt, J. P., Pletscher, L. S. & Cheverud, J. M. Genetic variation and
713   correlation of dietary response in an advanced intercross mouse line produced from two divergent
714   growth lines. *Genet. Res.* **85,** 211–222 (2005).
715   55. Mayo, L. M. *et al.* Conditioned preference to a methamphetamine-associated contextual cue in
716   humans. *Neuropsychopharmacol. Off. Publ. Am. Coll. Neuropsychopharmacol.* **38,** 921–929 (2013).
717   56. Graham, F. K. Presidential Address, 1974. The more or less startling effects of weak prestimulation.
718   *Psychophysiology* **12,** 238–248 (1975).
719   57. Grabowski, P. P., Morris, G. P., Casler, M. D. & Borevitz, J. O. Population genomic variation reveals
720   roles of history, adaptation and ploidy in switchgrass. *Mol. Ecol.* **23,** 4059–4073 (2014).
721   58. DePristo, M. A. *et al.* A framework for variation discovery and genotyping using next-generation DNA
722   sequencing data. *Nat. Genet.* **43,** 491–498 (2011).
723   59. Korneliussen, T. S., Albrechtsen, A. & Nielsen, R. ANGSD: Analysis of Next Generation Sequencing
724   Data. *BMC Bioinformatics* **15,** 356 (2014).
725   60. Browning, S. R. & Browning, B. L. Rapid and Accurate Haplotype Phasing and Missing-Data
726   Inference for Whole-Genome Association Studies By Use of Localized Haplotype Clustering. *Am. J.*
727   *Hum. Genet.* **81,** 1084–1097 (2007).
728   61. Browning, B. L. & Browning, S. R. Genotype Imputation with Millions of Reference Samples. *Am. J.*
729   *Hum. Genet.* **98,** 116–126 (2016).
730   62. Han, L. & Abney, M. Identity by descent estimation with dense genome-wide genotype data. *Genet.*
731   *Epidemiol.* **35,** 557–567 (2011).

63. Abney, M. Identity-by-descent estimation and mapping of qualitative traits in large, complex pedigrees. *Genetics* **179,** 1577–1590 (2008).

64. Wise, A. L., Gyi, L. & Manolio, T. A. eXclusion: toward integrating the X chromosome in genome-wide association analyses. *Am. J. Hum. Genet.* **92,** 643–647 (2013).

65. Chang, C. C. *et al.* Second-generation PLINK: rising to the challenge of larger and richer datasets. *GigaScience* **4,** 7 (2015).

66. Joo, J. W. J., Hormozdiari, F., Han, B. & Eskin, E. Multiple testing correction in linear mixed models. *Genome Biol.* **17,** 62 (2016).

67. Han, B., Kang, H. M. & Eskin, E. Rapid and accurate multiple testing correction and power estimation for millions of correlated markers. *PLoS Genet.* **5,** e1000456 (2009).

68. Zhou, X. & Stephens, M. Efficient multivariate linear mixed model algorithms for genome-wide association studies. *Nat. Methods* **11,** 407–409 (2014).

69. Schroeder, A. *et al.* The RIN: an RNA integrity number for assigning integrity values to RNA measurements. *BMC Mol. Biol.* **7,** 3 (2006).

70. Degner, J. F. *et al.* Effect of read-mapping biases on detecting allele-specific expression from RNA-sequencing data. *Bioinforma. Oxf. Engl.* **25,** 3207–3212 (2009).

71. Wang, X. & Clark, A. G. Using next-generation RNA sequencing to identify imprinted genes. *Heredity* **113,** 156–166 (2014).

72. Kim, D., Langmead, B. & Salzberg, S. L. HISAT: a fast spliced aligner with low memory requirements. *Nat. Methods* **12,** 357–360 (2015).

73. Lawrence, M. *et al.* Software for computing and annotating genomic ranges. *PLoS Comput. Biol.* **9,** e1003118 (2013).

74. Aken, B. L. *et al.* The Ensembl gene annotation system. *Database J. Biol. Databases Curation* **2016,** (2016).

75. Anders, S. & Huber, W. Differential expression analysis for sequence count data. *Genome Biol.* **11,** R106 (2010).

76. Pickrell, J. K. *et al.* Understanding mechanisms underlying human gene expression variation with RNA sequencing. *Nature* **464,** 768–772 (2010).

77. Davis, J. R. *et al.* An Efficient Multiple-Testing Adjustment for eQTL Studies that Accounts for Linkage Disequilibrium between Variants. *Am. J. Hum. Genet.* **98,** 216–224 (2016).

78. Friddle, C. J. *et al.* High-throughput mouse knockouts provide a functional analysis of the genome. *Cold Spring Harb. Symp. Quant. Biol.* **68,** 311–315 (2003).

79. Brunschwig, H. *et al.* Fine-scale maps of recombination rates and hotspots in the mouse genome. *Genetics* **191,** 757–764 (2012).

End Notes

Author contributions: NMG maintained the AIL colony, phenotyped the mice, prepared RNA-sequencing libraries, and performed QTL/eQTL analysis under supervision of AAP and MA. AAP and MA also provided computational resources for the analyses in this paper. JS prepared RNA-sequencing data for eQTL mapping under supervision of SC. CLS assisted with colony maintenance, tissue collection, RNA extraction, and GBS. MGD performed experiments in mutant mice. AL, JSG and AIHC measured muscle and bone phenotypes. NMG co-wrote the manuscript with AAP, who designed the study.

787
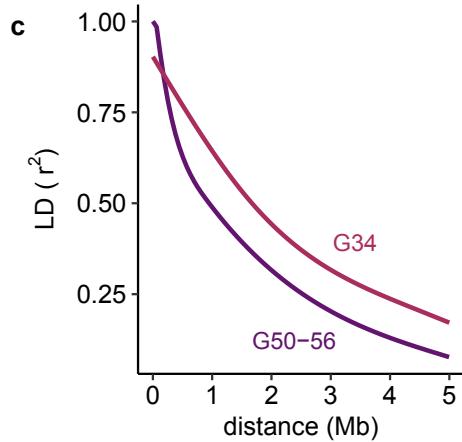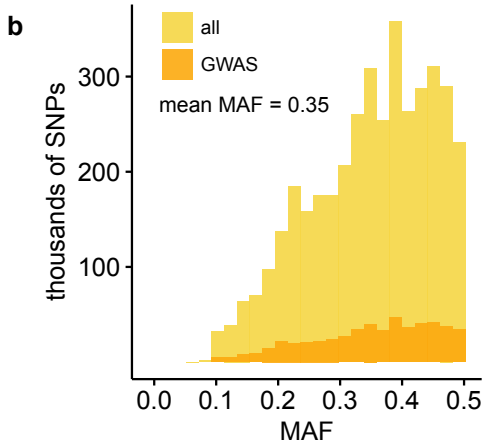788 **Conflict of interest:** The authors declare no conflict of interest.

789

Figure Legends

791
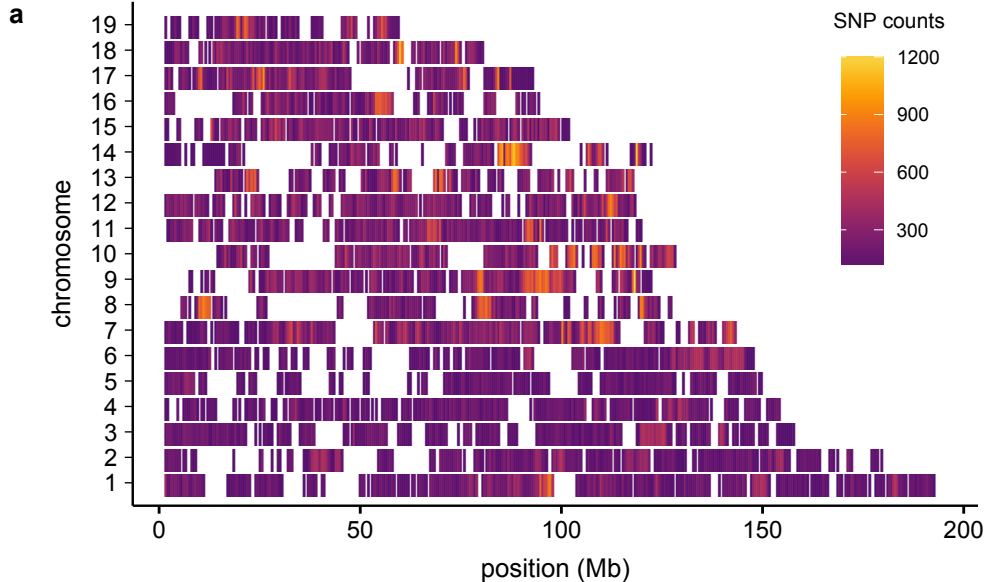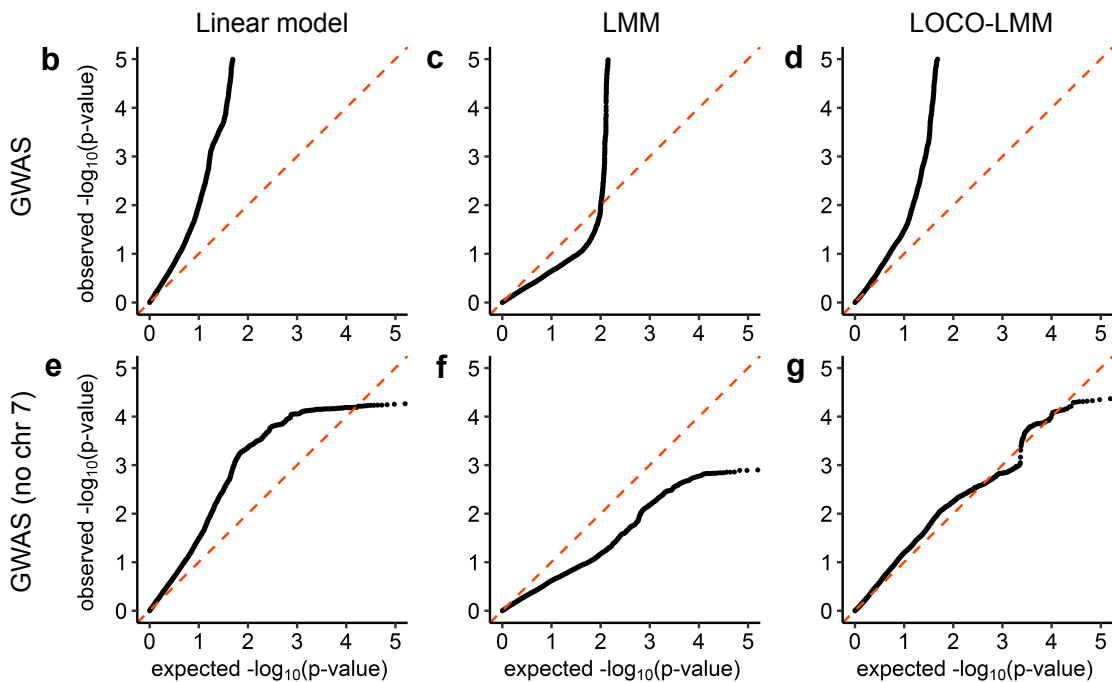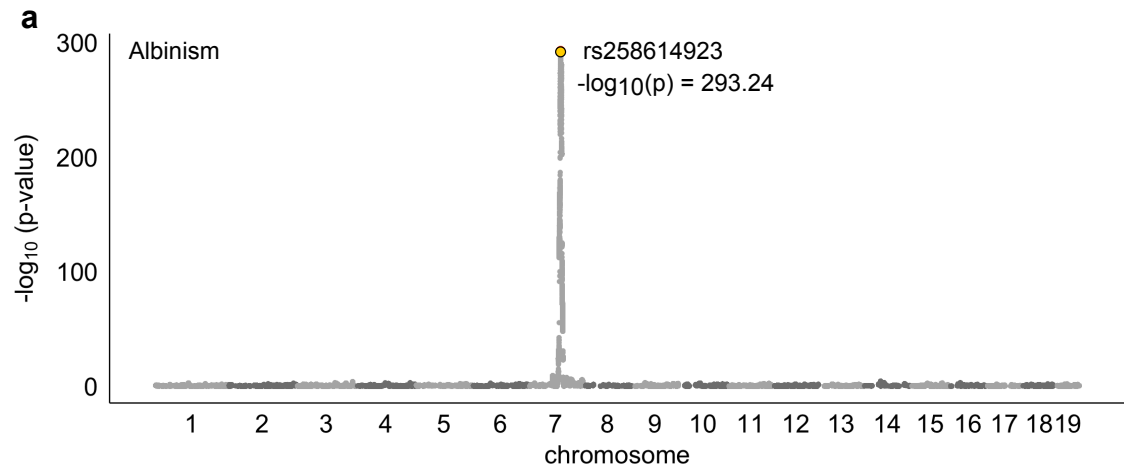792 **Figure 1. Variants, MAFs and LD decay in the LG x SM AIL.** Imputation provided 4.3 million SNPs. Filtering for
793 LD ($r^2 \geq 0.95$), MAF < 0.1, and HWE ($p \leq 7.62 \times 10^{-6}$) resulted in 523,028 SNPs for GWAS. **(a)** SNP distribution and
794 density of GWAS SNPs are plotted in 500 kb windows for each chromosome. As shown in **Supplementary Fig. 1**,
795 regions with low SNP density correspond to regions predicted to be nearly identical by descent in LG and SM
796 (Nikolskiy et al. 2015). **(b)** MAF distributions are shown for 4.3 million imputed SNPs (gold; unfiltered) and for the
797 523,028 SNPs used for GWAS (orange; filtered). Mean MAF is the same in both SNP sets. **(c)** Comparison of LD
798 decay in G50-56 (dark purple) and G34 (light purple) of the LG x SM AIL. Each curve was plotted using the 95th
799 percentile of r^2 values for SNPs spaced up to 5 Mb apart.
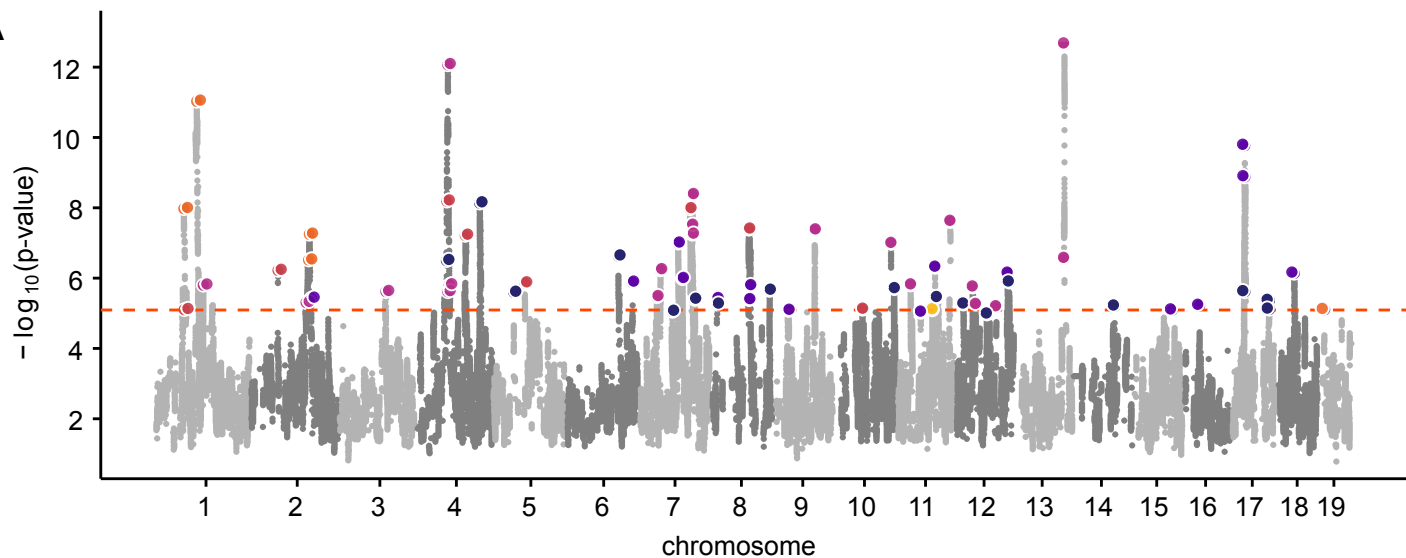
800
801 **Figure 2. GWAS for albinism verifies that the LOCO-LMM effectively controls type I and type II error.** We
802 conducted a GWAS for albinism, a Mendelian trait caused by the *Tyr^c* locus on mouse chromosome 7, using three
803 models: a linear model, an LMM, and a LOCO-LMM. We also repeated each scan after excluding SNPs on
804 chromosome 7. A Manhattan plot of results from the LOCO-LMM is shown in **(a)**. Quantile-quantile plots of
805 expected vs. observed p-values are shown for (**b**) a simple linear model that does not account for relatedness; **(c)** a
806 standard LMM that includes all GWAS SNPs in the GRM (i.e. the random effect); and **(d)** a LOCO-LMM whose
807 GRM excludes SNPs located on the chromosome being tested. Plots **(e-g)** show results after excluding
808 chromosome 7 from the GWAS.

809
810 **Figure 3. Manhattan plot and heritability for 120 traits measured in the LG x SM AIL.** We identified 126 loci for
811 behavioral and physiological traits using 1,063 mice from G50-56 of the LG x SM AIL. A Manhattan plot of GWAS
812 results is shown in **(a)**. Associations for related traits are grouped by color. For clarity, related traits that mapped to
813 the same locus (**Supplementary Table 1**) are highlighted only once. The dashed line indicates a permutation-
814 derived significance threshold of $-\log_{10}(p)=5.09$ ($p=8.06 \times 10^{-6}$; $\alpha=0.05$). **(b)** For a representative subset of traits, SNP
815 heritability estimates (percent trait variance explained by 523,028 GWAS SNPs) are shown. Precise estimates of
816 heritability with standard error are provided for all traits in **Supplementary Table 2**.

817
818 **Figure 4. Replication of an association between *Csmd1* and locomotor activity. (a)** Regional plot drawn from
819 all 4.3 million SNPs showing the association between rs33436747 and D5 activity levels. The location of Csmd1,
820 1.5-LOD interval (gold bar), areas of elevated recombination[79] (green plus symbols), regions predicted to be nearly
821 IBD between LG and SM[21] (grey bars), and SNP MAFs (grey heatmap) are indicated. Points are colored by LD (r^2)
822 with rs33436747. The dashed line indicates a significance threshold of $-\log_{10}(p)=5.09$ ($\alpha=0.05$). **(b)** PheWAS plot of
823 associations between rs33436747 and other behavioral traits measured in G50-56 mice. **(c)** Bar plot of quantile-
824 normalized residuals of locomotor activity at the Csmd1 locus are plotted for G50-56 mice. **(d)** Bar plot of quantile-
825 normalized residuals of locomotor activity at the Csmd1 locus for G34 mice[13]. rs33436747 was not genotyped in
826 G34; therefore, we plotted activity by genotype at the nearest SNP (rs33014260); 6,764 bp upstream of
827 rs33436747). **(e)** Plot of locomotor activity data (distance traveled in 0-30 min) for Csmd1 mutant mice. In panels
828 **(c-e)** the number of mice in each genotype class is shown below the corresponding bar. ANOVA and two-sided t-
829 test (95% confidence level) p-values are shown for each comparison.

16

a

SNP counts

b

thousands of SNPs

mean MAF = 0.35

all
GWAS

c

LD (r^2)

G34

G50−56

position (Mb)

chromosome

MAF

distance (Mb)

a Albinism

rs258614923
$-\log_{10}(p) = 293.24$

chromosome

Linear model   **LMM**   **LOCO-LMM**

GWAS

b   **c**   **d**

GWAS (no chr 7)

e   **f**   **g**

expected $-\log_{10}$(p-value)

A

B

A D5 activity (10-15 min)

rs33436747
$-\log_{10}(p)=5.29$

r^2

MAF

1.5-LOD

Nearly IBD in LG and SM

Csmd1

$4N_{er}/Kb$ 0.1+

chromosome 8 position (bp)

B rs33436747 (chr8:16,981,604)

p=5.09e-06

D5 activity (10-15 min)

p=0.05

D1 activity saline   D2 activity meth   D3 activity saline   D4 activity meth   D5 activity saline   D8 activity saline   PPI   startle

C Anova, p = 7.9e−06

0.00055

0.00011   0.11

555   405   76

LG   HET   SM

chr8:16,981,604 (rs33436747)
G50-56 (n=1,036)

D Anova, p = 3.5e−09

0.00021

6.7e−07   0.033

411   247   30

LG   HET   SM

chr8:16,974,840 (rs33014260)
G34 (n=688)

E Anova, p = 0.034

0.026

0.52   0.058

31   59   48

WT   HET   MUT

Csmd1 genotype (n=138)